Korean J. Chem. Eng., 40(9), 2187-2198 (2023)
DOI: 10.1007/s11814-023-1397-z

pISSN: 0256-1115
eISSN: 1975-7220

Anticorrosive efficiency and adsorption characteristics of natural plant gums on mild steel exposed to the Diesel/Saline water biphasic system

Raji Palanisamy*, Jayapriya Jayaprakash*,†, Duraisami Dhamodharan,***, and Hun-Soo Byun**,†**

*Department of Applied Science and Technology, AC Tech Campus, Anna University, Chennai
**Department of Chemical and Biomolecular Engineering, Chonnam National University, Yeosu, Jeonnam 59626, Korea
***Green Lab, Department of Prosthodontics, Saveetha Dental College and Hospitals,
Saveetha Institute of Medical and Technical Sciences, Chennai
(*Received 27 November 2022 • Revised 21 December 2022 • Accepted 31 January 2023*)

Abstract−Metallic equipment and structures that come in contact with a variety of petroleum products, solvents, water, the atmosphere, and soil in the oil and gas industry are highly prone to a range of corrosion phenomena, which escalate the risk of serious accidents. The use of green corrosion inhibitors in oil and gas can significantly reduce the maintenance and service costs. This study focuses on the anti-corrosive behavior of natural exudate gums, such as *Azadirachta indica* (G1), *Moringa oleifera* (G2), *Prosopis juliflora* (G3) and *Prunus dulcis* (G4). These gums were evaluated as corrosion inhibitors on mild steel against the diesel/saline water biphasic system by the weight loss method and electrochemical techniques. The inhibition efficiency was high at 93.86, 95.75, 92.42, and 90.02% at the highest tested concentration (5,000 ppm) for the gums G1, G2, G3, and G4, respectively. Among the investigated natural gums, the lowest corrosion rate (29.36 mm yr^{-1}) and highest inhibition efficiency (95.75%) were achieved with *Moringa oleifera* (G2) at 5,000 ppm. The activation energy of the corrosion inhibition process (4.00-38 $kJmol^{-1}$) was higher than that of the uninhibited system (1.8 $kJmol^{-1}$), indicating that the inhibited systems possessed higher energy barriers and followed the Langmuir adsorption process. Our corrosion test results validate that the *Moringa oleifera* gum can serve as an effective eco-friendly corrosion inhibitor for mild steel in the biphasic system of diesel/saline water.

Keywords: Corrosion, Mild Steel, Diesel/Waster Biphasic Medium, Natural Gums, Inhibitor

INTRODUCTION

Corrosion involves the inevitable damage to metals and nonmetals because of their physical, chemical, or electrochemical interactions with aggressive environments such as acidic/alkaline conditions [1]. Rusting, a common type of corrosion, is caused by the formation of metal oxides (e.g., Fe_2O_3) in metals and iron alloys exposed to oxygen and moisture for a prolonged duration [2]. However, in anoxic conditions, the reduction of water regulates the corrosion process, and generates hydrogen and hydroxide ions ($2H_2O+2e^- \Leftrightarrow H_2(g)+2OH^-$; $Fe_{(s)}+2OH^- \Leftrightarrow Fe(OH)_{2(s)}+2e^-$), which transforms metals to metal oxides via the Schikorr reaction ($3Fe(OH)_{2(s)} \Leftrightarrow Fe_3O_{4(s)}+H_{2(g)}+2H_2O$) [3]. Corrosion is a serious and challenging issue worldwide, with negative impacts on economic growth, health, safety, technological development, and cultural heritage (metallic artifacts).

The establishment of oil and gas reserves under aggressive environments causes the corrosion of drilling equipment involved in large-scale, hydrocarbon extraction and fuel transport [4]. The pipelines used in the oil and gas sector come in contact with several substances, including crude oils, natural gas, petroleum products, fuels, solvents, water, the atmosphere, and soil and, therefore, are highly vulnerable to a variety of corrosion phenomena, which can result in serious accidents [5]. The corrosion of metal components in under storage systems and diesel pipelines is very common. Internal corrosion is usually caused in an environment that contains water with sodium chloride (salt), carbon dioxide, and/or hydrogen sulfide [6]. Pipeline deterioration occurs in such an environment predominantly due to iron dissolution and subsequent strength reduction. Similarly, during the transport of diesel by sea lanes, ships use ballast tanks for diesel storage. To maintain the stability of the ship, a system must be designed such that the fuel in the reactor can counterbalance the seawater. To achieve this, the consumed fuel in the reactor must automatically be replenished to compensate for the weight loss. However, saline wastewater remains at the bottom of the tank during the fuel refilling process, causing fuel contamination and corrosion of the tank surface in contact with the oil-saline water mixture [7,8].

The estimated global cost of corrosion annually is 2.5 trillion US dollars, which equals 3-4% of the global GDP. As per the National Association of Corrosion Engineers (NACE), the US refineries spend more than 3.7 billion dollars annually towards corrosion-related repairs [9]. When appropriate mitigation methods are not followed in petroleum industries, different forms of corrosion, such as uniform, galvanic, crevice, pitting and stress corrosion, are commonly initiated. These can result in plant shutdown, loss of product in pipelines, product contamination and/or reduced process efficiency, while also incurring additional maintenance costs for the repair or

†To whom correspondence should be addressed.
E-mail: jayapriyachem@gmail.com, hsbyun@jnu.ac.kr

replacement of corroded parts [10].

The most common corrosion inhibitors employed in the petroleum industry are nitrogenated-compounds, including amine salts, ammonium salts, imidazoline and their derivatives [11-13]. However, these inhibitors are synthetic and expensive chemicals, which are also very hazardous to the environment. Newer green approaches involving biopolymers, such as chitosan, pectin and plant gums, have been tested for carbon steel corrosion mitigation [14]. Natural gums are hydrophilic polysaccharides which consist of D-galactose, D-arabinose, D-rhamnose, D-xylose, D-galacturonic acid, L-rhamnose and L-fructose. These heterocyclic compounds possess oxygen heteroatoms (O-glycosidic bonds), which aids their adsorption on the metal surface, thereby protecting it against corrosion [15]. Abdallah [16] were the first to study the anticorrosive characteristics of guar gum on carbon steel (CS), and they used 1 M H_2SO_4 containing sodium chloride as the corrodent. The maximum inhibition efficiency (93%) was obtained at 1,500 ppm of the gum concentration, which also acted as a mixed inhibitor [16]. Later, guar gum-grafted polyacrylamide (GG-g-PAM) was tested against mild steel corrosion in 1 M HCl, and the highest inhibition efficiency (CIE) up to 93% was observed after 5 h of incubation [17]. Some other natural exudate gums, such as *Pachylobus edulis (*PE) gum, *Raphia hookeri* gum (RhG), *Carob gum* and *Azadirachta indica* (AIG) gum, have been tested as corrosion inhibitors in highly acidic condition [18-20].

Most gums have -COOH functional groups; they can easily form complexes with metal ions and on the metal surfaces. Hence, the corrosion inhibition efficiency of these natural gums depends mainly on the functional groups of the inhibitor molecule, steric factors, aromaticity, electron density at the donor atoms and the electronic structure [21]. Different gums have been reported as efficient anticorrosive agents for mild steel in acidic environments; however, these gums have not yet been tested as corrosion inhibitors in oil/water biphasic systems. A shortage of information on thermodynamic parameters and adsorption characteristics associated with such corrosion inhibitors limited its applications in industry. Considering the great demand for green corrosion inhibitors, this work can provide solutions to some of the relevant problems, such as uncontrolled hydration rate, pH-dependent solubility, thermal instability and algal and microbial contamination, which are associated with use of natural gums as corrosion inhibitors in the oil/gas industry.

Hence, this study investigates the natural exudate gums from *Azadirachta indica* (G1), *Moringa oleifera* (G2), *Prosopis juliflora* (G3) and *Prunus dulcis* (G4) on the corrosion behavior of mild steel exposed to a biphasic diesel/saline water system based on weight loss, electrochemical impedance, and potentiodynamic polarization tests. Further, the adsorption behavior and thermodynamic characteristics of mild steel corrosion, including activation energy (E), enthalpy (H), entropy (S) and free energy changes (G), were also evaluated in the biphasic diesel/saline water system.

MATERIALS AND METHODS

1. Material

Natural plant gums from *Azadirachta indica* (G1), *Moringa oleifera* (G2), *Prosopis juliflora* (G3) and *Prunus dulcis* (G4) were used as green inhibitorsin this study. These gum samples were obtained from various locations in Kallakkurichi district, Tamil Nadu, India by making incisions on the bark of the respective trees and tapping the resin. After collection, the samples were completely dehydrated by direct sun-drying for over two weeks and ground using a mortar and pestle to obtain fine powders. The gum powders were stirred in distilled water for 3 h, and the partially solubilized samples were strained through a fine mesh to separate the macroscopic residue. The soluble polysaccharides in the filtered mixture were precipitated with excess ethanol (ethanol/water ratio - 8 : 2). Then, the precipitates were dried, finely powdered and stored in a desiccator. For the experiments, the powdered gums were added to distilled water to obtain the desired concentrations from 100 ppm to 5,000 ppm.

The composition of mild steel coupons employed in the corrosion test was 0.15% C, 0.25% Si, 0.03% S, 0.015% Al, 0.25% Cu and the rest Fe. The coupons used for the weight loss analysis were cut into 14.5×1.8 cm^2 strips. For electrochemical studies, coupons with an exposed area of 11.56 cm^2 were used as the working electrodes. Before each test, the sample surface was mechanically abraded using emery papers of various grades up to 1,500 and cleaned with ethanol and subsequently with distilled water before drying. A biphasic corrosive medium (50 mL Diesel+150 mL of 2% NaCl solution) was used in all experiments.

2. Gravimetric Measurements

The corrosion rate was estimated by dipping the mild steel coupons in the unstirred corrosive medium without or with the different natural gums at varying concentrations for 24 h at room temperature. After immersion for 24 h, the coupons were retrieved, rinsed with acetone and water and then dried. The weight loss due to corrosion was computed after immersion. The corrosion rate (CR) was determined as below [22]:

$$\text{Corrosion rate}\left(\frac{\text{mm}}{\text{year}}\right) = 87{,}600 \times \frac{\Delta W}{\rho A T} \quad (1)$$

where ΔW, ρ, T and A are the average loss of material (g), density (g/cm^3), immersion time (24 h), and surface area of the sample (11.56 cm^2), respectively. The corrosion inhibition efficiency (IE %) was evaluated as follows:

$$EI\% = \frac{(CR_{G0} - CR_{GI})}{CR_{G0}} \times 100 \quad (2)$$

where CR_{GI} and CR_{G0} are the corrosion rates on the material with and without the addition of the green inhibitor, respectively [23]. The surface coverage (θ) of the inhibitors on the coupon surface was calculated as [24]

$$\theta = \frac{\text{Inhibition Efficiency}}{100} \quad (3)$$

3. Electrochemical Measurements

The electrochemical analyses involved using a Vertex 1A electrochemical workstation (Ivium Technologies, Netherlands). In the electrochemical cell, a platinum foil, a saturated calomel electrode, and the tested mild steel specimen were utilized as the auxiliary, reference, and working electrodes, respectively.

3-1. Electrochemical Impedance Spectroscopy (EIS)

The electrochemical impedance spectra were recorded in the 10 kHz to 10 mHz frequency range at an amplitude of 10 mV. The obtained impedance data were analyzed using ZSimpWin software. The inhibition efficiency (IE%) was obtained using the charge transfer resistance (R_{ct}) values given by the Nyquist plots as follows:

$$\text{Inhibition efficiency} = \left(\frac{R_{ct(GI)} - R_{ct(G0)}}{R_{ct(GI)}}\right) \times 100 \quad (4)$$

where $R_{ct(GI)}$ and $R_{ct(G0)}$ represent the charge transfer resistance in the presence and absence of the inhibitor, respectively [25].

3-2. Potentiodynamic Polarization

The potentiodynamic polarization experiments were carried out in the potential range of −1,000 mV to +1,000 mV versus the open-circuit potential at a 1 mV/s scan rate with specimens immersed for 24 h in the test solution for at room temperature. Subsequently, the Tafel plots were drawn to explore the Tafel parameters, namely corrosion rate and corrosion current. The I_{corr} was used in the following equation to calculate the inhibition efficiency.

$$\text{Inhibition efficiency} = \left(\frac{I_{corr(G0)} - I_{corr(GI)}}{I_{corr(G0)}}\right) \times 100 \quad (5)$$

where $I_{corr(G0)}$ and $I_{corr(GI)}$ denote the current values in the absence and presence of an inhibitor, respectively.

4. Surface Analysis

4-1. Fourier Transform Infrared (FTIR) Spectroscopy

The Fourier transform infrared (FTIR) spectra of the inhibitors and the mild steel surfaces exposed to the inhibitors for 24 h were recorded in the 4,000-500 cm^{-1} wavenumber range using a Bruker instrument with a resolution of 4 cm^{-1}. After 24 h, the immersed coupons were taken out, cleaned with water and dried at room temperature. The green inhibitor adsorbed on the surface of the coupons was pelletized with KBr for FTIR spectroscopy.

4-2. Microscopic Studies

The surfaces of the mild steel coupons exposed to the inhibitors were investigated by a scanning electron microscope (Hitachi TM-1000) equipped with an EDAX at an accelerating voltage of 15 kV to identify the major morphological changes, which can help in the cursory evaluation of the types of corrosion phenomena (e.g., uniform, pitting, etc.) occurring at different conditions [26].

5. Adsorption Studies

To determine the interaction at the interface of the natural corrosion inhibitors and the mild steel surface, various adsorption isotherm models, such as Langmuir (L-A), Temkin (T-A), Freundlich (F-A), Frumkin, El Awad (F-E-A), and Flory-Huggins adsorption (F-H-A) models, were fitted [27]. The surface coverage (θ) was estimated from the inhibition efficiency obtained from the gravimetric measurements.

$$\theta = \frac{\text{Inhibition Efficiency}}{100} \quad (6)$$

The equations of the various models used in this study are given below:

(a) Langmuir Model

$$\frac{CR}{\theta} = \frac{1}{K_{ads}} + CR \quad (7)$$

(b) Temkin Model

$$\theta = \frac{-2.303\log K_{ads}}{2a} - \frac{-2.303\log C_{inh}}{2a} \quad (8)$$

(c) Freundlich Model

$$\log\theta = \log K_{ads} + n\log CR \quad (9)$$

(d) Frumkim

$$\log\left[CR\left(\frac{\theta}{1-\theta}\right)\right] = 2a\theta + 2.303\log K_{ads} \quad (10)$$

(e) El-Awady's thermodynamic/kinetic adsorption isotherm

$$\log\left(\frac{\theta}{1-\theta}\right) = y\log CR + \log K_{ads} \quad (11)$$

(f) Flory-Huggins adsorption isotherm

$$\log\left(\frac{\theta}{CR}\right) = b\log(1-\theta) + \log K_{ads} \quad (12)$$

where K_{ads}- adsorption constant and CR- corrosion rate in mm yr^{-1}.

RESULTS AND DISCUSSION

1. Weight Loss Measurement

The corrosion rates on the mild steel surface caused by the corrosive diesel/saline water biphasic medium containing various concentrations of the natural gums were investigated based on weight loss after 24 h of immersion at room temperature to evaluate the corrosion inhibition efficiency of the gums. The corrosion rate ($mmyr^{-1}$), corrosion inhibition efficiency (%) and surface coverage (θ) were calculated as per the formulas mentioned in section 2.2 (Table 1).The corrosion rate on the metal declined as the gum concentration was increased from 100 to 5,000 ppm for all the analyzed gums. This happens since the gum molecules adsorbed on the metal surface act as an electron transfer barrier, thereby facilitating corrosion inhibition. This suggests that the inhibition efficiency is concentration dependent. It was also found that the inhibitor concentration greatly influences the extent of protection offered by them against corrosion of the metal. The inhibition efficiencies were high, reaching 93.86, 95.75, 92.42, and 90.02% at the highest concentration (5,000 ppm) of the gums G1, G2, G3, and G4, respectively. The extent of protection offered by the gums against corrosion is proportional to the metallic surface area masked by the adsorbed gum molecules. In our experiments, the surface coverage of the inhibitor increased with the inhibitor concentration. Among the selected natural gums, the lowest corrosion rate (29.36 $mmyr^{-1}$) and the highest inhibition efficiency (95.75%) were achieved with G2 at 5,000 ppm.

Notably, the corrosion rate dramatically decreased by 8.62, 11.58, 3.67 and 3.77-fold in the presence of gums G1, G2, G3, and G4, even at low concentrations of 5,000 ppm compared with the uninhibited corrosive medium (339.88 $mmyr^{-1}$). The surface coverage parameter (θ) denotes the fraction of the mild steel surface area covered by adsorbed gum molecules. The surface coverage values were determined using Eq. (3), and the values of surface coverage are given in Table 1. This suggests the strong adsorption of inhibitors on the metallic surface through gum components, such as arabinogalactan, sucrose, oligosaccharides, polysaccharides and gluco-

Table 1. Corrosion parameters obtained from weight loss of Mild steel in 150 ml (2% of NaCl solution)+50 ml of diesel biphasic medium in the absence and the presence of various concentrations of Gums

Azadirachta indica (G1)											
Concentration (ppm)	Blank	100	200	300	400	500	1,000	2,000	3,000	4,000	5,000
Efficiency at 25 °C (%)		73.92	76.53	81.56	83.19	85.22	86.93	89.56	91.68	93.34	93.86
CR at 25 °C (mmpy)	339.88	191.86	186.23	137.55	110.61	95.73	87.28	65.56	55.51	42.64	39.42
Surface coverage θ at 25 °C		0.74	0.76	0.81	0.83	0.85	0.87	0.89	0.92	0.93	0.93
Moringa oleifera (G2)											
Concentration (ppm)	Blank	100	200	300	400	500	1,000	2,000	3,000	4,000	5,000
Efficiency at 25 °C (%)		71.82	73.99	76.49	77.54	80.92	83.28	86.73	89.68	93.34	95.75
CR at 25 °C (mmpy)	339.88	185.83	177.78	156.06	148.02	127.91	113.83	90.90	82.86	45.05	29.36
Surface coverage θ at 25 °C		0.72	0.74	0.76	0.77	0.81	0.83	0.87	0.9	0.93	0.96
Prosopis juliflora (G3)											
Concentration (ppm)	Blank	100	200	300	400	500	1,000	2,000	3,000	4,000	5,000
Efficiency at 25 °C (%)		61.59	66.09	68.79	71.24	76.94	78.78	80.75	84.86	86.94	92.42
CR at 25 °C (mmpy)	339.88	279.14	263.05	226.05	224.44	150.43	139.17	126.70	98.95	87.28	49.47
Surface coverage θ at 25 °C		0.62	0.66	0.69	0.71	0.77	0.79	0.81	0.85	0.87	0.92
Prunus dulcis (G4)											
Concentration (ppm)	Blank	100	200	300	400	500	1,000	2,000	3,000	4,000	5,000
Efficiency at 25 °C (%)		63.50	65.35	67.17	73.95	75.04	79.31	82.64	85.65	87.70	90.02
CR at 25 °C (mmpy)	339.88	248.17	240.53	219.21	173.36	163.70	139.57	115.84	94.52	81.65	80.85
Surface coverage θ at 25 °C		0.63	0.65	0.67	0.74	0.75	0.79	0.83	0.86	0.88	0.90

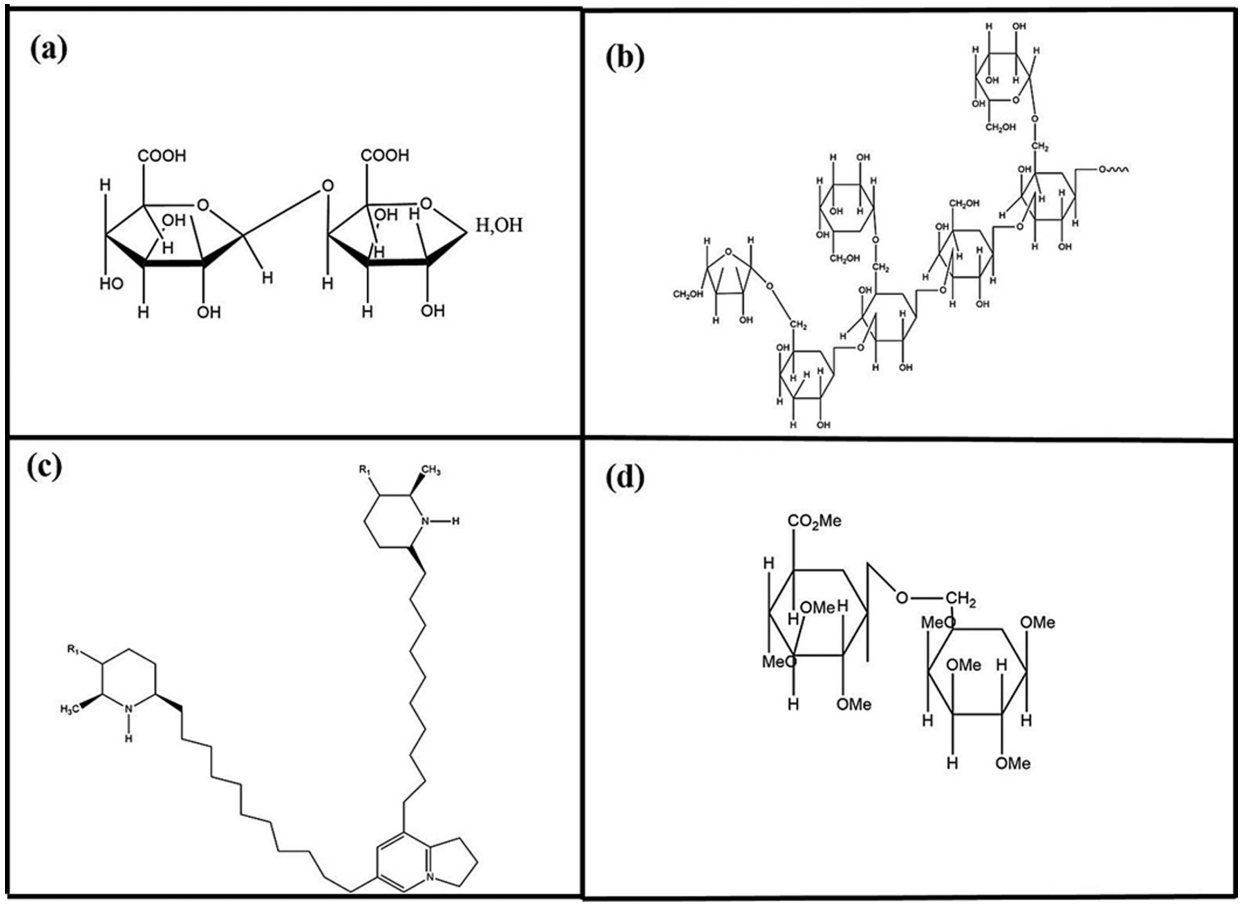

Fig. 1. Chemical structure of (a) *Azadirachta indica* (G1), (b) *Moringa oleifera* (G2), (c) *Prosopis juliflora* (G3) and (d) *Prunus dulcis* (G4).

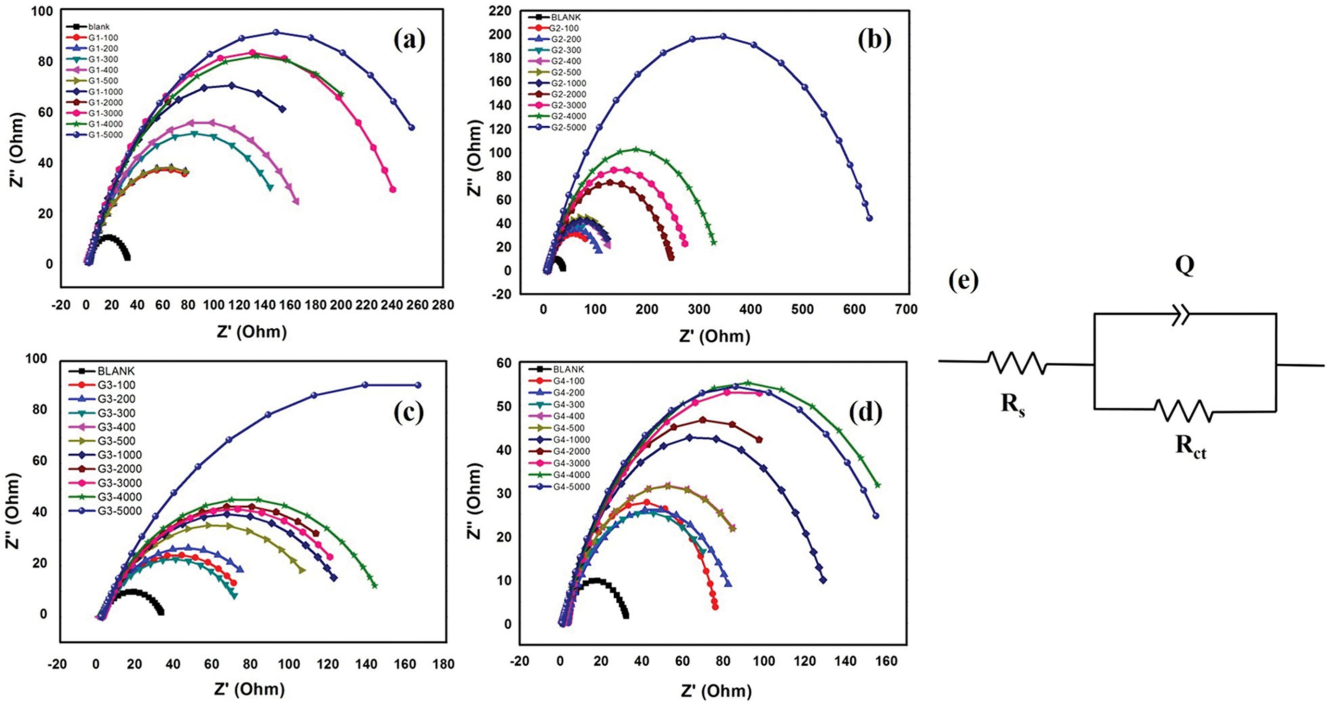

Fig. 2. Nyquist plots recorded at open circuit potentials for Mild steel in 150 ml (2% of NaCl solution)+50 ml of diesel biphasic medium in the absence and presence of different concentrations of (a) *Azadirachta indica* (G1), (b) *Moringa oleifera* (G2), (c) *Prosopis juliflora* (G3) and (d) *Prunus dulcis* (G4). (e) Equivalent circuit used for Electrochemical studies at 25 °C after 24 h of immersion.

proteins, which contain heteroatoms like oxygen and nitrogen. The adsorption of the inhibitory molecules on the metal surface also depends on the number of electron-donating functional groups, such as -OH, -COOH and -NH groups, available for bond formation, leading to the mitigation of corrosion shown in Fig. 1.

2. Electrochemical Impedance Spectroscopy Studies

The EIS spectra of mild steel in the biphasic diesel/saline water corrosive medium without and with the inhibitors are presented in Fig. 2(a)-(d) to predict the R_{ct}. The impedance spectra were further examined by fitting them using a Randles equivalent circuit in the ZSimpWin software, as shown in Fig. 2(e), and the chi-square values were found to be around 10^{-3}. The components in the equivalent circuit model are solution resistance (R_s), charge transfer resistance (R_{ct}) and a constant phase element (CPE; Q_c). A single and depressed semicircle loop was observed in the Nyquist plots Fig. 2(a)-(d) for mild steel corroded by the biphasic medium irrespective of the presence of the natural inhibitors. This is a typical characteristic of a corrosion process controlled by the charge transfer mechanism on a metal surface. It was observed that the diameters of the capacitive loops of the studied inhibitors at a low concentration (100 ppm) in the Nyquist plot were larger (R_{ct}=117.3, 106, 69.03, and 73.36 ohm cm^2 for G1, G2, G3 and G4, respectively) than that of the uninhibited system (R_{ct}=34.11 ohm cm^2).

The influence of inhibitor concentration on the corrosion inhibition efficiency is shown in Fig. 2(a)-(d). Larger semicircles were observed for the media with high gum concentrations at 5,000 ppm for G1 (R_{ct}=281.1 ohm cm^2); G2 (R_{ct}=650 ohm cm^2); G3 (R_{ct}= 294.7 ohm cm^2); G4 (R_{ct}=170.8 ohm cm^2) than those at the lower concentration of 100 ppm. The maximum inhibition efficiency (94.7%) was observed for G2 at 5,000 ppm concentration, while G1 showed 86.6% inhibition efficiency at 3,000 ppm. A further increase in G1 concentration to 5,000 ppm led to a maximum efficiency of only 87%. Even in the other cases, increasing the concentration of the selected gums greater than the respective optimal level did not alter the inhibition efficiency even by 1%. The high charge transfer resistance values are indicative of a slower corrosion process. In detail, these values suggest that the protective film thickness was enhanced due to the adsorption of more gum molecules at higher concentrations, causing larger surface areas to be masked by the gum molecules in the corrosive medium. At 5,000 ppm of gum G2, the value of charge transfer resistance was 650 ohm cm^2, and the inhibition efficiency approached 94.7%. This was also demonstrated by the weight loss method, thus verifying the strong adsorption of the *Moringa oleifera* gum (G2) on the metal surface.

The EIS data were analyzed using a simple Randle's equivalent circuit. A constant phase element was used in place of the capacitance in this work, and an interfacial capacitance was adopted to represent the non-ideal capacitive behavior of the inhibitor film and corrosion product formed on the metal surface. The impedance of CPE (Z_Q) is given below.

$$Z_Q = Y_0^{-1}(j\omega)^{-n} \quad (13)$$

where Y_0 is the CPE constant, n is the CPE exponent, j is an imaginary number, and w is the angular frequency. In general, the coefficient n falls in the range $-1 \le n \le 1$. The CPE would function as an inductor when n=−1, a resistor when n=0, a Warburg impedance when n=0.5, and a capacitor when n=1. A small value of n also refers to a rough surface. Table 2 shows that n<1 for all

Table 2. Electrochemical parameters and corresponding inhibition efficiency for corrosion of the of Mild steel in 150 ml (2% of NaCl solution)+50 ml of diesel in the biphasic medium in the absence and the presence of various concentrations of Gums

Azadirachta indica (G1)											
Concentration (ppm)	Blank	100	200	300	400	500	1,000	2,000	3,000	4,000	5,000
R_s (Ω cm^2)	1.19	1.76	1.77	1.72	0.99	1.79	1.85	1.84	1.66	1.87	1.68
R_{ct} (Ω cm^2)	34.11	117.3	119.8	166.9	181.3	203.3	212.3	236.2	256.0	269.5	281.1
n	0.70	0.70	0.70	0.73	0.70	0.70	0.74	0.73	0.70	0.73	0.70
$Q\times10^{-2}$ s^n (cm^2/ Ω)	6.67	4.40	3.94	3.92	1.38	1.19	1.09	0.68	0.61	0.61	0.41
C_{dl} (mF/cm^2)	94.9	89.0	76.7	68.9	20.4	17.3	14.7	8.14	7.47	7.36	4.39
Inhibition efficiency (%)		70.92	71.53	79.56	81.18	83.22	83.93	85.56	86.67	87.34	87.46
Degree of surface coverage (θ)		0.71	0.71	0.79	0.81	0.83	0.84	0.85	0.87	0.87	0.87
Moringa oleifera (G2)											
Concentration (ppm)	Blank	100	200	300	400	500	1,000	2,000	3,000	4,000	5,000
R_s (Ω cm^2)	1.19	1.32	1.40	2.63	1.39	1.59	1.39	2.89	1.64	1.96	1.84
R_{ct} (Ω cm^2)	34.11	106	110	124	134	136	138	239	277	320	650
n	0.7	0.8	0.75	0.70	0.70	0.73	0.70	0.70	0.70	0.70	0.70
$Q\times10^{-2}$ s^n (cm^2/ Ω)	6.67	4.96	3.47	2.06	1.49	1.35	1.09	0.25	0.18	0.15	0. 09
C_{dl} (mF/cm^2)	94.9	75.06	54.16	30.79	20.0	16.88	13.03	2.0	1.31	1.11	0.70
Inhibition efficiency (%)		67.82	68.99	72.49	74.54	74.92	75.28	85.73	87.68	89.34	94.75
Degree of surface coverage (θ)		0.68	0.69	0.72	0.74	0.75	0.75	0.86	0.88	0.89	0.95
Prosopis juliflora (G3)											
Concentration (ppm)	Blank	100	200	300	400	500	1,000	2,000	3,000	4,000	5,000
R_s (Ω cm^2)	1.19	1.51	1.40	0.83	1.28	1.45	1.79	1.70	2.02	1.53	1.46
R_{ct} (Ω cm^2)	34.11	69.03	87.66	94.19	107.4	117.4	130.1	135.1	135.7	282.9	294.7
n	0.7	0.7	0.7	0.7	0.7	0.7	0.75	0.7	0.7	0.7	0.7
$Q\times10^{-2}$ s^n (cm^2/ Ω)	6.67	4.24	2.62	2.01	1.89	1.29	1.29	0.82	0.78	0.60	0.30
C_{dl} (mF/cm^2)	94.9	67.09	37.33	26.44	25.65	15.38	15.29	8.64	7.99	7.6	2.87
Inhibition efficiency (%)		50.59	61.09	63.78	68.24	70.94	73.78	74.75	74.86	87.94	88.42
Degree of surface coverage (θ)		0.5	0.61	0.64	0.68	0.71	0.74	0.75	0.75	0.88	0.88
Prunus dulcis (G4)											
Concentration (ppm)	Blank	100	200	300	400	500	1,000	2,000	3,000	4,000	5,000
R_s (Ω cm^2)	1.19	3.99	2.65	0.94	0.88	0.88	1.57	1.46	1.50	0.84	0.82
R_{ct} (Ω cm^2)	34.11	73.36	86.03	90.18	103.2	103.5	132.8	140	159.8	168	170.8
n	0.70	0.70	0.70	0.70	0.70	0.70	0.71	0.75	0.70	0.70	0.72
$Q\times10^{-2}$ s^n (cm^2/ Ω)	6.67	3.38	3.20	2.61	2.28	2.27	1.09	0.98	0.82	0.72	0.50
C_{dl} (mF/cm^2)	94.9	49.79	49.41	37.75	32.85	32.75	12.63	10.8	9.25	7.92	4.77
Inhibition efficiency (%)		53.5	60.35	62.17	66.95	67.04	74.31	75.63	78.65	79.7	80.03
Degree of surface coverage (θ)		0.53	0.6	0.62	0.67	0.67	0.74	0.76	0.79	0.8	0.8

selected inhibitors represents the non-ideal capacitance behaviour of mild steel due to electrode surface heterogeneity. Table 2 shows that n<1 for all selected inhibitors represents the non-ideal capacitance behavior of mild steel due to electrode surface heterogeneity.

The double-layer capacitance (C_{dl}) was evaluated using the equation,

$$C_{dl}=\sqrt[n]{Q_{dl}\times R_{ct}^{(1-n)}} \quad (14)$$

For a non-ideally polarized electrode in which charge transfer primarily controls the corrosion. In this work, the double-layer capacitance was low (Table 2) in the inhibited corrosive medium compared to that in the uninhibited solution (94 $mFcm^{-2}$). For the best inhibitor (G2), the 67.82% inhibition efficiency at a low concentration of 100 ppm increased to 94.75% at the highest concentration of 5,000 ppm; however, the double-layer capacitance decreased by a hundred-fold. The double-layer capacitance values of all the inhibited media were lower (G1 - 4.39 $mFcm^{-2}$; G2 - 0.704 $mFcm^{-2}$; G3 - 2.87 $mFcm^{-2}$; G4 - 4.77 $mFcm^{-2}$) than that of the uninhibited solution (94 $mFcm^{-2}$) for their respective highest inhibition efficiencies (G1 - 87.46%; G2 - 94.75%; G3 - 88.42%; G4 - 80.03%), strongly suggesting the presence of a protective film on the metal surface. It can be inferred that the increase in double layer thickness caused by inhibitor adsorption decreased the capacitance [28,29]. From Table 2, it can be seen that the *Moringa oleifera* gum at a concentration of 5,000 ppm had the lowest double-layer capacitance (0.704 $mFcm^{-2}$) of all inhibitors, providing strong

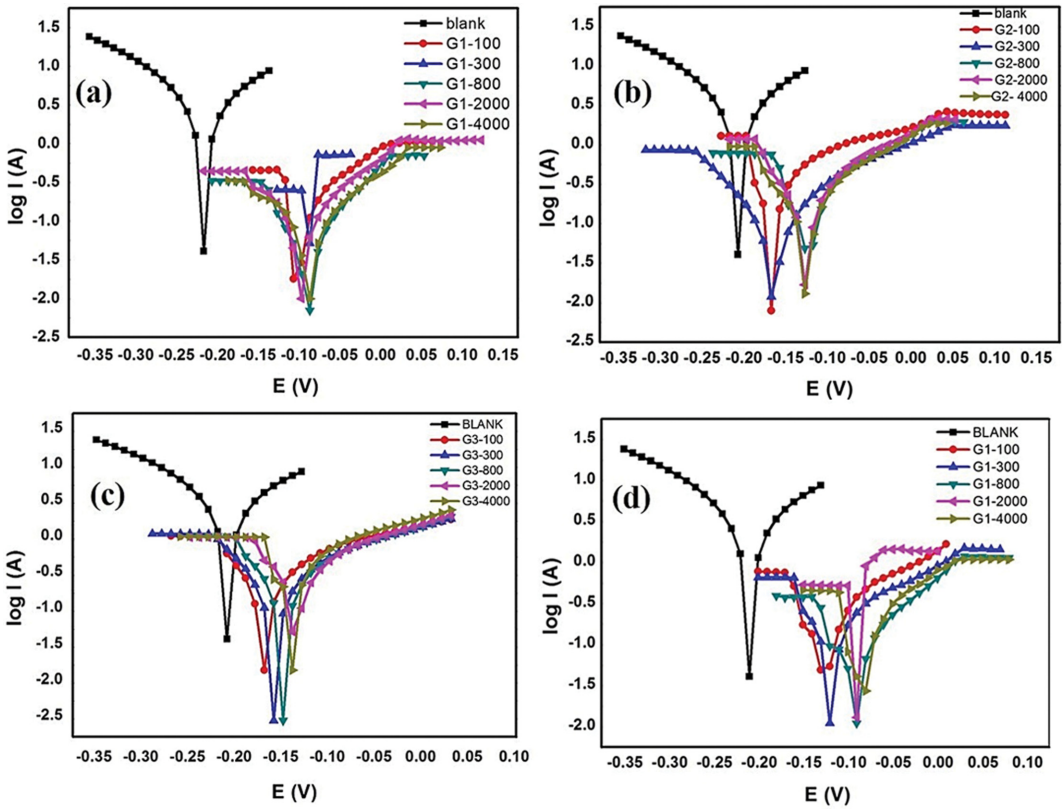

Fig. 3. Polarisation curves for Mild steel in 150 ml (2% of NaCl solution)+50 ml of diesel biphasic medium in the absence and presence of different concentrations of (a) *Azadirachta indica* (G1), (b) *Moringa oleifera* (G2), (c) *Prosopis juliflora* (G3) and (d) *Prunus dulcis* (G4). at 25 °C after 24 h of immersion.

evidence for a dense and thick adsorbed film on the surface.

3. Potentiodynamic Polarization Studies

The polarization curves of mild steel in the biphasic diesel/saline water corrosive medium without and with the natural gums (inhibitors) at room temperature are presented in Fig. 3(a)-(d). All the selected inhibitors displayed a shift towards the anodic domain of the polarization curves, leading to lower current density values compared with the blank (without inhibitor). This suggests that the selected natural gums could inhibit the steel dissolution reactions. The electrode potential (E) and the logarithm of current (log i) of an electrode demonstrate a linear relationship when polarized to sufficiently large potentials, both in anodic and cathodic directions. The range in which the electrode exhibits such a relationship is called the Tafel region. The anodic and cathodic curves were extrapolated to find the polarization parameters, including corrosion current density (I_{corr}), corrosion potential (E_{corr}), and the anodic and cathodic Tafel slopes (β_a and β_c). The electrochemical corrosion parameters derived using the Tafel method is listed in Table 3. To ascertain the corrosion-protective effect of the gums, their corrosion inhibition efficiency (%) was determined using Eq. (5) and the corrosion current densities evaluated by the Tafel extrapolation method, as shown in Table 3.

The polarization results match the gravimetric measurements reported in this work, signifying the improvement of inhibition efficiency with increasing gum concentration. Table 3 demonstrates that the corrosion currents obtained for mild steel in media containing the inhibitors at 5,000 ppm (0.007 $mAcm^{-2}$ for G1, 0.003 $mAcm^{-2}$ for G2, 0.012 $mAcm^{-2}$ for G3 and 0.004 $mAcm^{-2}$ for G4) were lower than that of the blank (0.221 $mAcm^{-2}$). The maximum efficiency of 98.70% was observed for G2 at 5,000 ppm. Based on the weight loss method, we also found that gum G2 was the best. The trend of corrosion inhibition efficiency was the same, but some differences were observed in the corrosion rate probably because the weight loss method provides average corrosion rates, while the polarization method yields the instantaneous corrosion rates (Table 1 and Table 3).

As seen in Table 3, the lowest corrosion rates (0.93 $mmyr^{-1}$, 0.28 $mmyr^{-1}$, 0.46 $mmyr^{-1}$ and 0.79 $mmyr^{-1}$, respectively) and the highest inhibition efficiency (64.14, 89.36, 82.19, and 69.58%, respectively) of G1, G2, G3 and G4 were achieved at 100 ppm. Further, increasing the gum concentration from 100 to 5,000 ppm caused the corrosion rate to decrease in all tested cases owing to the better protection offered by the gums at higher concentration. Among the investigated gums, G2 acts as the best corrosion inhibitor in the diesel/saline water biphasic medium because it strongly adsorbs to the mild steel surface and blocks the sites, thereby decreasing the diffusion rate of corrosive reactants to the metal surface and thereby shielding the metal from corrosion. It is known that if the E_{corr} value changes by more than ±85 mV vs SCE in comparison with the corrosion potential of the blank, the selected inhibitor can be considered cathodic- or anodic-type.

In contrast, a change in the values of both β_a and β_c in the pres-

Table 3. Potentiodynamic polarization parameters of the of Mild steel in 150 ml (2% of NaCl solution)+50 ml of diesel in the biphasic medium in the absence and the presence of various concentrations of Gums

Azadirachta indica (G1)											
Concentration (ppm)	Blank	100	200	300	400	500	1,000	2,000	3,000	4,000	5,000
$-E_{corr}$ mV	235.2	158.8	112.2	94.6	93.3	87.4	79.6	76.9	64.2	52.6	30.1
i_{corr} mA	2.56	0.92	0.86	0.50	0.27	0.27	0.25	0.20	0.08	0.08	0.08
i/A mA/cm^2	0.22	0.08	0.07	0.04	0.02	0.02	0.02	0.02	0.01	0.01	0.01
β_a V/dec	0.46	0.23	0.18	0.16	0.12	0.11	0.08	0.08	0.04	0.03	0.13
β_c V/dec	0.21	5.73	4.69	3.53	1.83	1.68	0.36	0.14	0.09	0.04	0.02
CR mm/year	2.61	0.93	0.88	0.51	0.27	0.27	0.25	0.20	0.08	0.08	0.08
Efficiency %	------	64.14	66.38	80.37	89.44	89.59	90.3	92.14	96.79	96.79	96.83
Moringa oleifera (G2)											
Concentration (ppm)	Blank	100	200	300	400	500	1,000	2,000	3,000	4,000	5,000
$-E_{corr}$ mV	235.2	215.9	209.4	204.9	188.5	184.8	180.3	144.9	142.7	142.3	142.3
i_{corr} mA	2.56	0.27	0.22	0.18	0.16	0.15	0.14	0.12	0.11	0.08	0.03
i/A mA/cm^2	0.22	0.02	0.02	0.01	0.01	0.01	0.01	0.01	0.01	0.01	0.002
β_a V/dec	0.46	0.23	0.23	0.22	0.20	0.18	0.15	0.14	0.13	0.13	0.01
β_c V/dec	0.21	0.10	0.09	0.08	0.08	0.06	0.05	0.04	0.04	0.04	0.04
CR mm/year	2.61	0.28	0.20	0.19	0.17	0.15	0.14	0.13	0.11	0.08	0.03
Efficiency %	------	89.36	92.5	92.82	93.55	94.25	94.52	95.12	95.73	96.75	98.7
Prosopis juliflora (G3)											
Concentration (ppm)	Blank	100	200	300	400	500	1,000	2,000	3,000	4,000	5,000
$-E_{corr}$ mV	235.2	217.0	204.2	202.4	193.9	187.6	184.4	171.9	168.1	159.3	150.9
i_{corr} mA	2.6	0.46	0.38	0.35	0.30	0.29	0.29	0.23	0.15	0.15	0.14
i/A mA/cm^2	0.22	0.04	0.03	0.03	0.03	0.02	0.02	0.02	0.01	0.01	0.01
β_a V/dec	0.46	0.30	0.27	0.26	0.23	0.22	0.22	0.20	0.20	0.19	0.17
β_c V/dec	0.21	0.08	0.07	0.06	0.06	0.05	0.05	0.05	0.05	0.03	0.03
CR mm/year	2.61	0.46	0.35	0.39	0.30	0.30	0.29	0.23	0.15	0.15	0.15
Efficiency %	------	82.19	86.38	85.12	88.38	88.52	88.76	91.11	94.08	94.13	94.38
Prunus dulcis (G4)											
Concentration (ppm)	Blank	100	200	300	400	500	1,000	2,000	3,000	4,000	5,000
$-E_{corr}$ mV	235.2	142.9	131.4	103.2	101.5	101.1	98.9	94.4	97.6	86.4	16.7
i_{corr} mA	2.6	0.78	0.57	0.45	0.39	0.14	0.11	0.11	0.10	0.06	0.05
i/A mA/cm^2	0.22	0.07	0.05	0.04	0.03	0.01	0.01	0.01	0.01	0.004	0.004
β_a V/dec	0.46	0.20	0.18	0.17	0.14	0.14	0.13	0.11	0.09	0.09	0.07
β_c V/dec	0.21	2.05	1.06	1.02	0.07	0.05	0.04	0.04	0.04	0.03	0.01
CR mm/year	2.61	0.79	0.58	0.46	0.40	0.15	0.11	0.11	0.10	0.06	0.05
Efficiency %	------	69.58	77.62	82.22	84.65	94.33	95.6	95.8	96.15	97.78	97.95

ence of inhibitors indicates that the inhibitor controls both metal dissolution and the kinetics of hydrogen evolution. As seen in Fig. 3, the corrosion potential demonstrated a gradual shift towards anodic potential with respect to the blank with increasing inhibitor concentration, revealing that the rate of the cathodic reaction had minimal effect on the rate of corrosion. From Fig. 3(a)-(d) it is evident that adding the gums at varying concentrations to the biphasic diesel/saline water system changed the shape of the cathodic and anodic curves, probably due to the differences in their adsorption capacity, which is dependent on the molecular structure of the respective gums.

4. FTIR and SEM Characterization

Fig. 4 shows the FTIR spectra of the natural gums used as corrosion inhibitors in this study. The intense peaks at 2,800-3,000 and 3,000-3,600 cm^{-1} originate, respectively, from the C-H and O-H stretching vibrations. Adsorption peaks at 2,975 and 2,966 cm^{-1} correspond to the C-H bond vibrations for all the gums except MO. The vibrational mode located at 2,975-2,966 cm^{-1} vanished completely in the MO spectrum; however, the MO gum polysaccharide showed a major band in the 3,277-3,000 cm^{-1} range corresponding to O-H stretching in the alcohol groups when compared to all selected gums. This suggests that some of the hydroxyl groups in the natural plant gums bonded with the metal surface by forming H-bonds. The absorption bands at around 800-1,200 cm^{-1} represent the stretching vibrations of the C-C, C-O, and C-O-C bonds, as well as the C-O-H bonds and C-H bending modes [30-32].

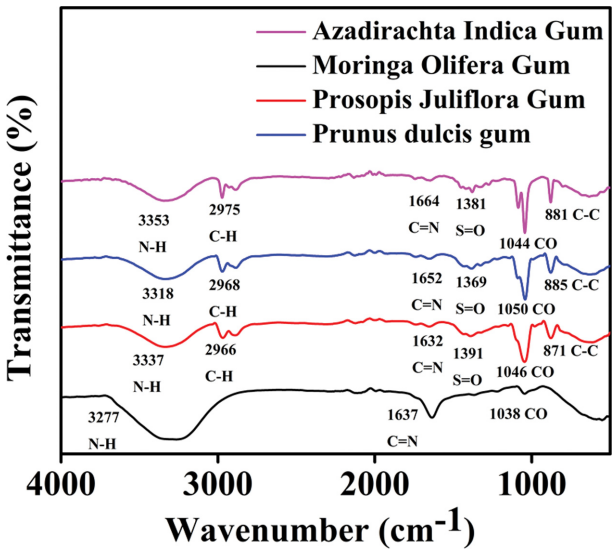

Fig. 4. FTIR spectra of *Azadirachta indica* (G1), *Moringa oleifera* (G2), *Prosopis juliflora* (G3) and *Prunus dulcis* (G4).

Polygalacturonic acids exhibit absorption maxima in this region; absorption at 1,038-1,044 cm^{-1} unveils the presence of galactose-containing polysaccharides in the selected gums. The carboxylic acid (COOH) groups are denoted by the typical in-plane O-H bending mode peak at 1,664 cm^{-1}, which shows the highest intensity in the MO gum spectrum compared with all the other gums. This indicates that the presence of numerous functional groups, including hydroxyl (-OH), carboxylic (COOH) and heteroatoms (O), in the molecular structure of the selected gums, inhibits the anodic/cathodic reactions either by electrostatic adsorption on the metal surface or coordinate-type linkages with the partially filled Fe orbital [15].

Fig. 5 shows the SEM analysis of the mild steel surfaces after immersion in the biphasic diesel/water corrosive medium containing 5,000 ppm inhibitor (G2) for 24 h. The surface of mild steel was smooth when immersed in the corrosive medium with inhibitors; however, surface pits were clearly seen on mild steel placed in the uninhibited medium (Fig. 5(d)-(f)). Pitting corrosion may be occurring on the metal surface. Meanwhile, the EDX spectrum of the steel samples in the corrosive media shows a high atomic percentage of oxygen, confirming the formation of corrosion products, while in the presence of G2, the spectra show lower intensity peaks for oxygen atoms (Fig. 5(g)-(i)), indicating that the natural gum (G2) formed a surface-protective layer to combat corrosion. The white patches on the metal surfaces exposed to the inhibitor

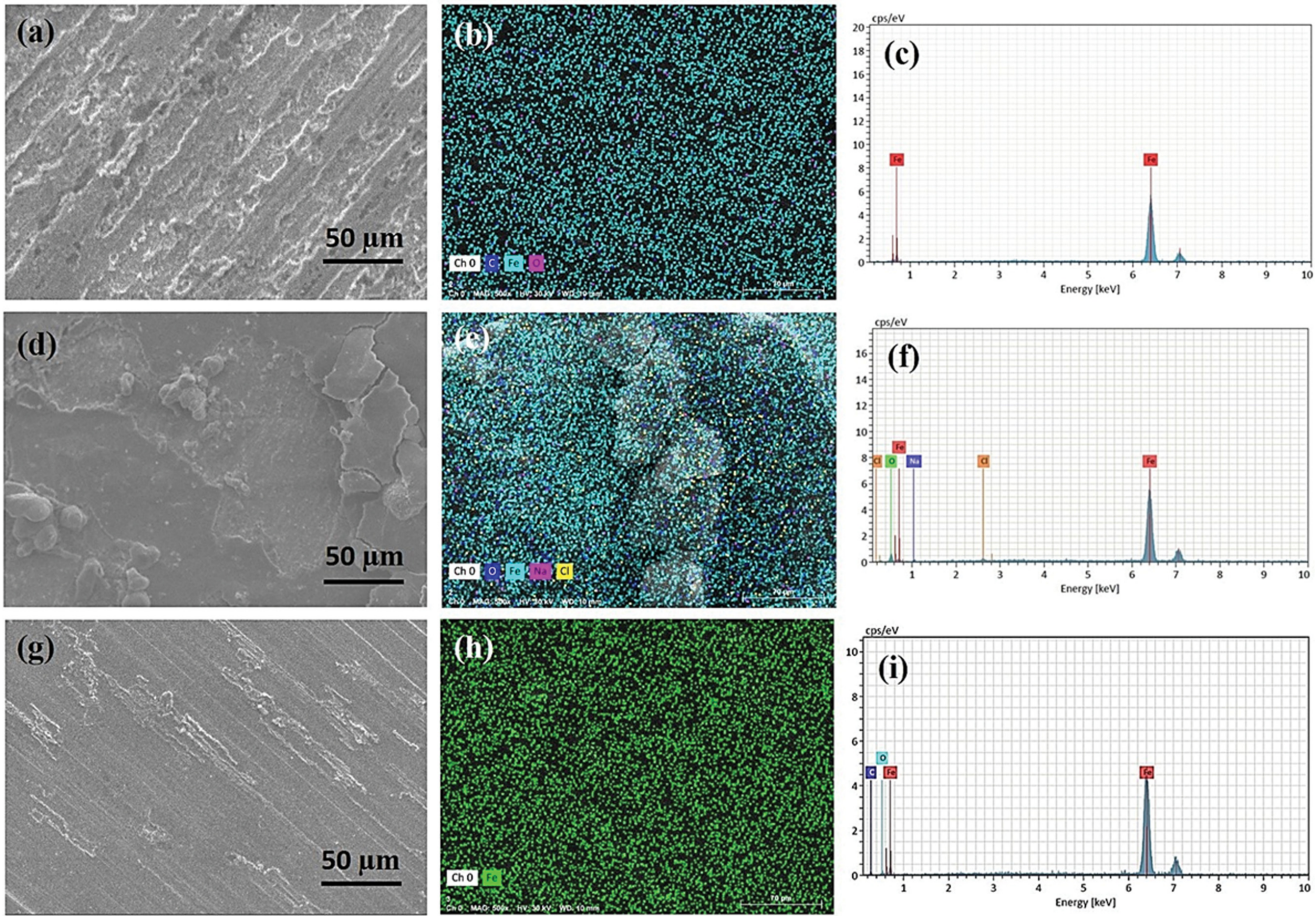

Fig. 5. SEM and EDX analysis of Mild steel surface of (a), (b), (c) Mild steel (Bare) surface's (d), (e), (f) corrosion without inhibition, (g), (h), (i) corrosion with inhibition of gum for 24 hr.

Table 4. R^2 values for the various adsorption isotherms considered for Mild Steel in 150 ml (2% of NaCl solution)+50 ml of diesel in the biphasic medium in the absence and the presence of various concentrations of Gums

	Langmuir		Temkin		Freundlich		Frumkin		El-Awadys		Flory Huggins	
Temperature °C	25	45	25	45	25	45	25	45	25	45	25	45
Azadirachta indica (G-1)	0.99	0.99	0.95	0.96	0.94	0.96	0.96	0.97	0.97	0.95	0.97	0.94
Moringa oleifera (G-2)	0.99	0.99	0.97	0.96	0.97	0.96	0.98	0.98	0.86	0.90	0.83	0.86
Prosopis juliflora (G-3)	0.99	0.99	0.96	0.94	0.96	0.96	0.98	0.97	0.92	0.90	0.88	0.86
Prunus dulcis (G-4)	0.99	0.99	0.97	0.93	0.96	0.90	0.98	0.95	0.97	0.95	0.95	0.94

solutions indicate that the gum molecules were adsorbed and masked the surface from the aqueous layer.

5. Adsorption Isotherms and Thermodynamic Considerations

The surface coverage values were matched to various adsorption isotherm models to study the interaction between the natural corrosion inhibitors and the metal surface. The reduction in metal dissolution rate caused by the surface-adsorbed inhibitors occurs via active site blockage depending on the chemical structure of the inhibitor, electrolyte type, charge state and metal type/properties. Of the adsorption models tested, the best fit was obtained for the Langmuir isotherm (R^2=0.99) for all four gums (Table 4) at different temperatures. The slope value in the Langmuir isotherm was close to unity at 25 °C, indicating that there was no interaction between the gum molecules on the active sites, and also at 45 °C. The correlation coefficients (R^2) were in the following ranges for the Temkin (0.93-0.96), Freundlich (0.90-0.96), Frumkin (0.95-0.98), E-A (0.90-0.95) and F-H (0.86-0.94) isotherm even at 45 °C, confirming that the adsorption process obeyed the Langmuir model. K_{ads} is the adsorption equilibrium constant obtained from the Langmuir model and it is given in Table 5.

Table 5. Thermodynamic parameters of Langmuir isotherm for the Mild steel in 150 ml (2% of NaCl solution)+50 ml of diesel in the absence and the presence of different concentrations gums

	K_{ads} mol^{-1}		ΔG KJ mol^{-1}	
R^2	25 °C	45 °C	25 °C	45 °C
Azadirachta indica (G1)	17.02	11.67	−14.44	−14.42
Moringa oleifera (G2)	9.46	7.23	−12.99	−13.15
Prosopis juliflora (G3)	7.70	6.25	−12.48	−12.76
Prunus dulcis (G4)	8.62	8.40	−12.76	−13.55

The adsorption equilibrium constant K_{ads} relative to the standard free energy ΔG_{ads} (kJ/mol) was calculated as

$$\Delta G_{ads} = -RT \ln (2\times 10\ K_{ads}) \quad (15)$$

where R is the universal constant of ideal gases, T is absolute temperature, and 20 refers to the saline water concentration in ppm.

Table 6. Activation parameters of the dissolution of Mild steel in 150 ml (2% of NaCl solution)+50 ml of diesel in the absence and presence of different concentrations of Gums

Azadirachta indica (G1)											
Concentration (ppm)	Blank	100	200	300	400	500	1,000	2,000	3,000	4,000	5,000
Activation Energy (E_a) (KJ/mol)	1.90	10.08	7.21	11.77	14.96	17.60	18.39	27.20	24.04	33.01	26.70
Entropy ΔS (J/mol/K)	−181.72	−144.1	−161.81	−151.79	−148.71	−146.01	−147.94	−135.23	−152.95	−144.1	−174.81
Enthalpy ΔH (KJ/mol)	−1.73	12.27	7.10	11.02	12.45	13.54	13.13	17.33	12.25	15.13	10.14
Moringa oleifera (G2)											
Concentration (ppm)	Blank	100	200	300	400	500	1,000	2,000	3,000	4,000	5,000
Activation Energy (E_a) (KJ/mol)	1.90	13.94	11.65	14.25	13.17	14.63	13.83	17.57	11.67	31.17	30.43
Entropy ΔS (J/mol/K)	−181.72	−122.15	−139.08	−132.53	−141.4	−142.56	−151.8	−148.71	−170.28	−145.63	−164.88
Enthalpy ΔH (KJ/mol)	−1.73	18.93	14.04	16.41	13.92	13.96	11.47	12.83	6.56	14.63	9.20
Prosopis juliflora (G3)											
Concentration (ppm)	Blank	100	200	300	400	500	1,000	2,000	3,000	4,000	5,000
Activation Energy (E_a) (KJ/mol)	1.90	5.50	4.01	8.03	7.79	15.91	15.83	15.35	21.45	22.29	37.68
Entropy ΔS (J/mol/K)	−181.72	−157.57	−170.66	−148.71	−150.64	−125.99	−131.77	−139.86	−129.08	−134.08	−121.75
Enthalpy ΔH (KJ/mol)	−1.73	6.59	3.00	10.24	9.70	18.46	16.96	14.79	18.53	17.26	21.66
Prunus dulcis (G4)											
Concentration (ppm)	Blank	100	200	300	400	500	1,000	2,000	3,000	4,000	5,000
Activation Energy (E_a) (KJ/mol)	1.90	9.69	5.12	7.24	7.09	6.75	10.24	13.72	16.03	19.74	16.43
Entropy ΔS (J/mol/K)	−181.72	−131.38	−165.66	−155.26	−164.88	−168.35	−157.96	−151.41	−152.18	−146.79	−157.57
Enthalpy ΔH (KJ/mol)	−1.73	14.98	4.92	8.42	6.43	5.59	9.14	11.55	11.73	13.58	10.39

Table 7. Comparison between the inhibition efficiency of some other reported gum inhibitor on steel in acidic medium with the present work

S. No	Inhibitor source	Metal	Medium	Concentration	Efficiency %	Reference
1	Gum Arabic	Mild Steel	1 M HCl	1.0 g L^{-1}	95.00	[35]
2	*Azadirachta indica*	Mild Steel	1 M HCl	60 ppm	92.11	[36]
3	Guar gum	Carbon Steel	1 M H_2SO_4	1,500 ppm	94.75	[16]
4	Pachylobus edulis-gum	Mild Steel	2 M H_2SO_4	0.5 g L^{-1}	65.53	[18]
5	Gum Tragacanth Powder	Mild Steel	1 N Sulphuric Acid	40 ppm	86.89	[37]
6	XG-g-PAM	Mild Steel	15% HCl	0.4 g L^{-1}	94.79	[38]
7	Guar gum	Aluminium	1 M HCl	0.4 g L^{-1}	82.83	[39]
8	*Azadirachta indica* (G1)	Mild Steel	2% of NaCl solution with diesel	5,000 ppm	87.46	Present study
9	*Moringa oleifera (*G2)	Mild Steel	2% of NaCl solution with diesel	5,000 ppm	94.75	Present study
10	*Prosopis juliflora* (G3)	Mild Steel	2% of NaCl solution with diesel	5,000 ppm	88.42	Present study
11	*Prunus dulcis* (G4)	Mild Steel	2% of NaCl solution with diesel	5,000 ppm	80.03	Present study

At 25 °C, the ΔG_{ads} values were −14.44, −12.99, −12.48, and −12.76 kJmol^{-1} for G1, G2, G3 and G4 and at 45°, the ΔG_{ads} value were −14.42, −13.15, −12.76 and −13.55 kJ mol^{-1} respectively. These negative values denote the spontaneous physical adsorption of the inhibitors on mild steel (Table 5).

It is known that free energy equal to or greater than −20 kJ mol^{-1} indicates a physical adsorption process facilitated by electrostatic interactions between the corrosion inhibitor and the metallic surface. Meanwhile, free energy values around or lower than −40 kJ mol^{-1} denote a chemisorption process involving the sharing or relocationof charge from the corrosion inhibitor to the metal surface, resulting in a coordinate metal bond. Table 5 displays that the calculated ΔG_{ads} fell in the −12 to −14 kJ mol^{-1} range, suggesting physical adsorption of selected gum molecules on the metal surface. Temperature is critical to the efficiency of natural corrosion inhibitors. The activation energy was determined as

$$\log\frac{CR_2}{CR_1}=\frac{E_a}{2.303R}\left(\frac{1}{T_1}-\frac{1}{T_2}\right) \quad (16)$$

Where CR_1 and CR_2 refer to the mild steel corrosion rates at temperatures T_1 (298 K) and T_2 (318 K), respectively, E_a is the activation energy, and R is the gas constant.

As shown in Table 6, the activation energy was higher for the corrosion inhibition processes than that the uninhibited system (1.89 kJ mol^{-1}) due to the thin film formed on the mild steel surface, which leads to a higher energy barrier in the inhibited systems. Further, the activation energy increased as the inhibitor concentration increased since the thickness of the film layer increased, escalating the barrier to diffusion of reactants and energy transfer.

The enthalpy change (ΔH) and entropy change (ΔS) values calculated at different gum concentrations and temperature are given in Table 6.

$$\log\frac{CR}{T}=\frac{-\Delta H}{2.303R}\left(\frac{1}{T}\right)+\left[\log\frac{R}{Nh}+\left(\frac{\Delta S}{2.303R}\right)\right] \quad (17)$$

where h is Planck's constant, N is Avogadro's number; ΔH is the enthalpy change evaluated from the slope $\frac{-\Delta H}{2.303R}$ of the plot of $\log\frac{CR}{T}$ against $\left(\frac{1}{T}\right)$ and the entropy changes; ΔS is the entropy change evaluated from the intercept $\left[\log\frac{R}{Nh}+\left(\frac{\Delta S}{2.303R}\right)\right]$ of the same plot.

The ΔH values were positive (Table 6) and low enthalpy of adsorption was observed in the range of 2-21 kJ mol^{-1} for all the gums (less than 40 kJ mol^{-1}), indicating that gum adsorption of the gum on the metal followed a physical adsorption process. However, the entropy change values were negative for all the selected gums. This indicates that disorderliness decreases when the reactants transform into the activated complex. Moreover, the negative ΔS values suggest that the formation of the passivation layer is the rate-controlling step. This result is consistent with the work by Sudhish and Eno [33]. Table 7 compares the ability of the natural gums to inhibit the corrosion on steel exposed to acidic conditions. This study demonstrates that the adsorption of the tested natural gums on mild steel exposed to the biphasic diesel/saline water system is feasible and occurs spontaneously via a physical process according to the Langmuir isotherm.

CONCLUSIONS

In summary, the anti-corrosive effect of natural gums from *Azadirachta indica* (G1), *Moringa oleifera* (G2), *Prosopis juliflora* (G3) and *Prunus dulcis* (G4) on mild steel exposed to the biphasic diesel/saline water system was studied. The corrosion rates dramatically decreased by 8.62, 11.58, 6.87 and 4.20 folds, respectively, in the presence of 5,000 ppm G1, G2, G3, and G4 gums compared with rate observed in the uninhibited corrosive medium (339.88 mmyr^{-1}). The EIS and Tafel electrochemical plots revealed increasing inhibition efficiency with gum concentration, suggesting that the degree of protection offered by the inhibitor is concentration dependent. The double-layer capacitances in all the inhibited media (G1 - 4.39 mFcm^{-2}, G2 - 0.704 mFcm^{-2}, G3 - 2.87 mFcm^{-2}, and G4 - 4.77 mFcm^{-2}) were less than that of the uninhibited solution (94.9 mFcm^{-2}) for their respective highest inhibition efficiencies (G1 - 87.46%; G2 - 94.75%; G3 - 88.42%; G4 - 80.03%), strongly evidencing the presence of a protective layer on the mild steel surface. Further research on the surface interactions, shelf-life and pH stability of the natural gums in the biphasic medium at different temperatures is necessary for the application of these natural cor-

rosion inhibitors at the industrial scale.

ACKNOWLEDGEMENTS

This work was supported by the National Research Foundation of Korea (NRF) grant funded by the Korean government (MSIT) (No. 2021R1A2C2006888).

CONFLICTS OF INTEREST

There are no declared conflicts of interest.

REFERENCES

1. C. Chandrasatheesh, J. Jayapriya and P. Prabunathan, *J. Polym. Environ.*, **30**, 1528 (2022).
2. C. Chandrasatheesh and J. Jayapriya, Biocorrosion. In Bioelectrochemical Interface Engineering, In: R. N. Krishnaraj, R. K. Sani Eds., John Wiley & Sons, Inc. NJ (2020).
3. H. El Hajj, A. Abdelouas, Y. El Mendili, G. Karakurt, B. Grambow and C. Martin, *Corrosion Sci.*, **76**, 432 (2013).
4. M. Iannuzzi, A. Barnoush and R. Johnsen, *npj Mater. Degrad*, **1**, 2 (2017).
5. P. Badida,Y. Balasubramaniam and J. Jayaprakash, *J. Nat. Gas Sci. Eng.*, **66**, 284 (2019).
6. U. Unueroh, G. Omonria, O. Efosa and M. Awotunde, *Niger. J. Technol.*, **35**, 317 (2016).
7. D. M. Frazaõ, I. R. De Melo, M. R. S. Vieira and S. L. U. Filho, *Mater. Res.*, **22**, 1 (2019).
8. K. M. Usher, A. H. Kaksonen, I. Cole and D. Marney, *Int. Biodeterior. Biodegrad.*, **93**, 84 (2014).
9. J. S. Lee, R. I. Ray and B. J. Little, NACE International, NACE-10074, San Antonio, Texas (2010).
10. A. H. Al-Moubaraki and I. B. Obot, *J. Saudi Chem. Soc.*, **25**, 101370 (2021).
11. P. Topilnitskij, *Chem. Chem. Technol.*, **1**, 45 (2007).
12. B. D. B. Tiu and R. C. Advincula, *React. Funct. Polym.*, **95**, 25 (2015).
13. N. A. Odewunmi, M. M. Solomon, S. A. Umoren and S. A. Ali, *ACS Omega*, **5**, 27057 (2020).
14. N. R. Vaidya, P. Aklujkar and A. R. Rao, *J. Coat. Technol. Res.*, **19**, 223 (2022).
15. M. Mobin, M. Rizvi, L. O. Olasunkanmi and E. E. Ebenso, *ACS Omega*, **2**, 3997 (2017).
16. M. Abdallah, *Portugaliae Electrochim. Acta*, **22**, 161 (2004).
17. P. Roy, P. Karfa, U. Adhikari and D. Sukul, *Corrosion Sci.*, **88**, 246 (2014).
18. S. A. Umoren and U. F. Ekanem, *Chem. Eng. Commun.*, **197**, 1339 (2010).
19. S. A. Umoren and E. E. Ebenso, *Pigment Resin Technol.*, **37**, 173 (2008).
20. A. A. Dalhatu, A. I. Sani, B. S. Sani and D. N. Sani, *Int. Res. J. Pure Appl. Chem.*, **17**, 1 (2019).
21. B. Thirumalairaj and M. Jaganathan, *Egyptian J. Pet.*, **25**, 423 (2016).
22. J. C. da Rocha, J. A. C. P. Gomes and E. D'Elia, *Mater. Res.*, **17**, 1581 (2014).
23. G. Palumbo, K. Berent, E. Proniewicz and J. Banaś, *Materials (Basel)*, **12**, 2620 (2019).
24. P. Kumari and M. Lavanya, *J. Bio- and Tribo-Corrosion*, **7**, 110 (2021).
25. S. Bashir, A. Thakur, H. Lgaz, I.-M. Chung and A. Kumar, *Surf. Interfaces*, **20**, 100542 (2020).
26. M. Messali, H. Lgaz, R. Dassanayake, R. Salghi, S. Jodeh, N. Abidi and O. Hamed, *J. Mol. Struct.*, **1145**, 43 (2017).
27. O. A. Akinbulumo, O. J. Odejobi and E. L. Odekanle, *Results in Mater.*, **5**, 100074 (2020).
28. F. El-Hajjaji, I. Merimi, L. El Ouasif, M. El Ghoul, R. Achour, B. Hammouti, M. E. Belghiti, D. S. Chauhan and M. A. Quraishi, *Port. Electrochim. Acta*, **37**, 131 (2019).
29. P. Singh, D. S. Chauhan, K. Srivastava, V. Srivastava and M. A. Quraishi, *Int. J. Ind. Chem.*, **8**, 363 (2017).
30. A. Rezaei, A. Nasirpour and H. Tavanai, *Food Hydrocolls*, **60**, 461 (2016).
31. D. Mudgil, S. Barak and B. S. Khatkar, *Int. J. Biol. Macromol.*, **50**, 1035 (2012).
32. P. D. Vasko, J. Blackwell and J. L. Koenig, *Carbohydr. Res.*, **23**, 407 (1972).
33. A. R. Rezaierod, A. R. Rahimi and M. Chaghazardi, *Anal. Bioanal. Electrochem.*, **6**, 657 (2014).
34. K. Azzaoui, E. Mejdoubi, S. Jodeh, A. Lamhamdi, E. Rodriguez-Castellón, M. Algarra, A. Zarrouk, A. Errich, R. Salghi and H. Lgaz, *Corrosion Sci.*, **129**, 70 (2017).
35. M. Manickam, D. Sivakumar, B. Thirumalairaj and M. Jaganathan, *Adv. Phys. Chem.*, **2016**, 1 (2016).
36. M. Abdallah, *Portugaliae Electrochim. Acta*, **22**, 161 (2004).
37. M. Manickam, M. Jaganathan and D. Sivakumar, *Int. J. Innovative Sci. Res. Technol.*, **2**, 8 (2017).
38. A. Biswas, S. Pal and G. Udayabhanu, *Appl. Surf. Sci.*, **353**, 173 (2015).
39. G. Palumbo, K. Berent, E. Proniewicz, J. Banaś, *Materials (Basel)*, **12**, 16 (2019).